Geotechnical Engineering Journal of the SEAGS & AGSSEA Vol. 51 No. 2 June 2020 ISSN 0046-5828

Model Vibration Tests on Piled Raft and Pile Group Foundations in Dry Sand

Anh-Tuan Vu[1], Tatsunori Matsumoto[2] and Kohei Kenda[3]
[1]Le Quy Don Technical University, Vietnam
[2]Kanazawa University, Japan
[3]Hazama-Ando Corporation, Japan
[1]E-mail: vuanhtuan@mta.edu.vn
[2]E-mail: matsumoto@se.kanazawa-u.ac.jp
[3]E-mail: shirasagisan5@gmail.com

ABSTRACT: In this research, the authors carried out vibration load tests on piled raft and pile group models to investigate dynamic behaviours of the foundations. Foundation models consisting of 6 piles, with or without batter piles, were used in the experiments. They were pile rafts (6PR and 6BPR) if the raft was in contact with ground surface, while they were pile groups (6PG and 6BPG) if the raft was not in contact with ground surface. To create dynamic load acting on the foundation, a vibro-hammer, placed on the raft, was used. The vibro-hammer can provide vibration load (active shaking) mainly in the vertical direction (called vertical loading) or in the vertical and horizontal directions simultaneously (called combination loading) by rotating two discs of eccentric mass synchronously in opposite directions or the same direction, respectively. Active shaking tests were conducted on 4 types of pile foundation models (6PR, 6BPR, 6PG and 6BPG) in a consistent dry sand ground. The experimental results indicate that the piled rafts are more effective foundation type to decrease settlement and inclination under dynamic loading than the pile groups.

KEYWORDS: Piled raft, Pile group, Dry sand, Model test, Dynamic load

1. INTRODUCTION

Pile foundations supporting structures such as machine foundations, bridges, buildings, wind turbines etc. are subjected to dynamic cyclic loads caused by machine operation load, traffic load, wind load, or wave load. If excessive displacements and/or inclination of a foundation structure are caused by the dynamic loads, the structure could be damaged and could not be used as in normal status. Hence, it is necessary to investigate behaviours of pile foundations under dynamic cyclic loading.

Recently, piled raft foundations have been applied to buildings more and more popularly to reduce average and/or differential settlement, e.g. Katzenbach et al. (1998), Poulos and Davids (2005), Poulos et al. (2011), Yamashita et al. (2011) and Watcharasawe et al. (2017). Experimental studies as well as numerical analyses on behaviours of piled raft foundation having vertical piles alone have been conducted, e.g. Randolph (1994), Horikoshi et al. (2003), Matsumoto et al. (2004), Reul (2004), Sawada and Takemura (2014), Unsever et al. (2014), Hamada et al. (2015), Unsever et al. (2017) and Ko et al. (2017).

A number of studies on batter piles were reported, e.g. Sadek and Isam (2004), Ghasemzadeh and Alibeikloo (2011), Goit and Saitoh (2013), and Isam et al. (2012). The researches investigated the behaviours of pile groups with batter piles (Sadek and Isam, 2004, Ghasemzadeh and Alibeikloo, 2011; Isam et al., 2012;) or single batter piles (Goit and Saitoh, 2013). An experimental study on behaviours of piled rafts having batter piles subjected to combination of vertical and static horizontal loading was carried out by Vu et al. (2017). Vu et al. (2018) conducted finite element analyses on pile foundations including pile group and piled raft having batter piles subjected to static horizontal loading.

There is few experimental study on behaviours of piled rafts having batter piles subjected to dynamic loading, especially active dynamic loading. Hence, in this research, the authors carried out vibration load tests on piled raft and pile group models in a dry sand ground to investigate dynamic behaviours of the foundations. The results of the experiments are presented and discussed in this paper.

2. DESCRIPTION OF EXPERIMENTS

2.1 Pile foundation models

Pile foundation models used in Vu et al. (2017) were used in the experiments of this study. The pile foundation models consist of 6 piles with or without batter piles and a raft as shown in Figure 1. The model piles are close-ended aluminium pipe piles having an outer diameter of 20 mm, a thickness of 1.1 mm and a total length of 285 mm. In battered pile foundations (6BPR and 6BPG), inclination angle of batter piles is set at 15 degrees. The rectangular duralumin raft has dimensions of 240 mm in length, 160 mm in width, and 30 mm in thickness. The top section of 30 mm of the pile is embedded in the raft, so that the effective pile length below the raft base is 255 mm. Pile positions are shown in Figure 2.

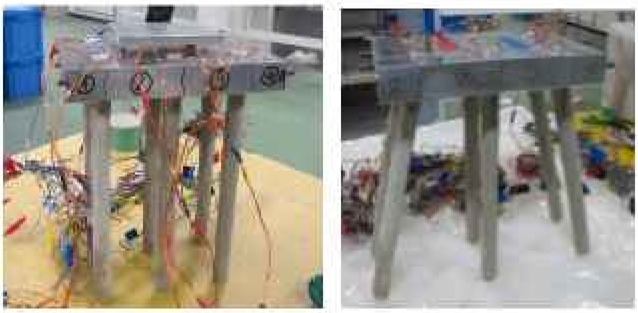

Figure 1 Pile foundation models

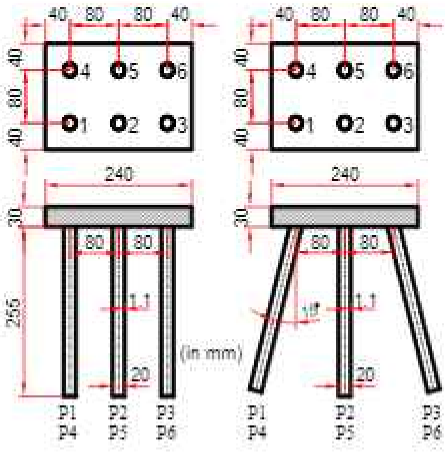

Figure 2 Dimensions of pile foundation models

Figure 3 shows cases of foundation type in the experiments. The foundation is a piled raft (PR) if the raft base is in contact with the ground surface. In the case of pile group (PG), a gap of 20 mm is set between the raft base and the ground surface. Each model pile is mounted with strain gauges along the pile shaft to obtain axial forces, shear forces, and bending moments of the pile. Note that axial forces and bending moments are calculated from measured axial strains, meanwhile shear forces are calculated from measured shear strains. The positions of strain gauges are shown in Figure 4. Physical and mechanical properties of the model pile are listed in Table 1.

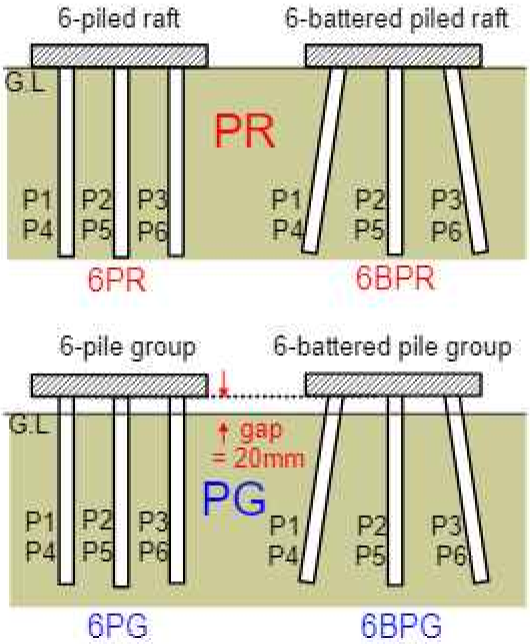

Figure 3 Cases of foundation type in the experiments

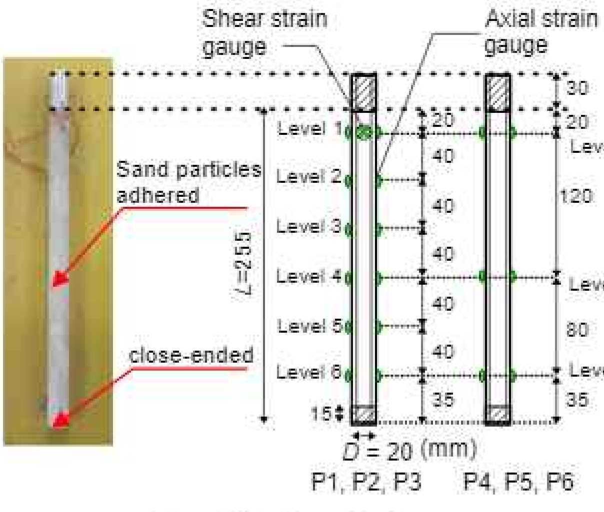

Figure 4 Positions of strain gauges

Table 1 Physical and mechanical properties of model pile

Property	Value
Outer diameter, D (mm)	20.00
Wall thickness, t (mm)	1.1
Length from raft base, L(mm)	255
Cross section area, A (mm^2)	65.31
Moment of inertia, I (mm^4)	2926.2
Young's modulus, E_p (N/mm^2)	70267
Poisson's ratio, ν	0.31

2.2 Model ground

The sand used for model ground in the experiments was dry silica sand #6 (water content w= 0.3%). The physical properties of the sand are shown in Table 2. The model ground with a relative density, D_r, of about 82% was prepared in a laminar box shown in Figure 5. The model ground consisted of 11 layers (10 layers of 50 mm and 1 layer of 30 mm). In order to control density of the model ground, the sand was compacted by tamping in each layer.

Table 2 Physical properties of silica sand #6

Property	Value
Density of soil particle, ρ_s (t/m^3)	2.668
Maximum dry density, ρ_{dmax} (t/m^3)	1.604
Minimum dry density, ρ_{dmin} (t/m^3)	1.269
Maximum void ratio, e_{max}	1.103
Minimum void ratio, e_{min}	0.663
Relative density, D_r (%)	82.0
Dry density, ρ_d (t/m^3)	1.533

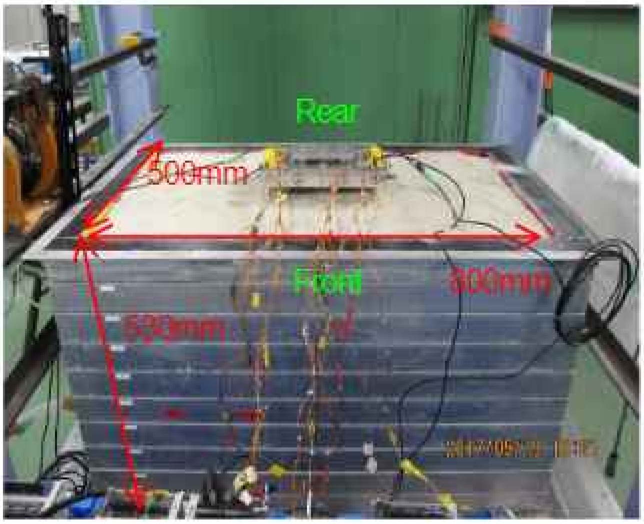

Figure 5 Dimension of laminar box

In order to grasp the mechanical behaviours of the sand, a series of consolidated drained (CD) triaxial compression tests were carried out (Vu et al, 2017). Five CD tests were carried out with different confining pressures, p_0, of 7, 17, 27, 50 and 100 kPa. The results of the CD tests are shown in Figure 6. The unloading and reloading steps were carried out at an axial strain of about 15% to estimate the unloading Young's modulus. The internal friction angle, ϕ_p', at peak strength is 42.8 degrees and the friction angle at residual state, ϕ_r', is 35 degrees. The initial stiffness, $\Delta q/\Delta\varepsilon_a$, increases almost linearly with increase in the square root of p_0. It is seen from Figure 6b that a small amount of negative dilatancy occurs at a very early stage of shearing followed by a large amount of positive dilatancy. Positive dilatancy behaviour weakens after the axial strain, ε_a, exceeds about 8%.

2.3 Loading equipment and measurement items

Figure 7 shows the initial state of a pile foundation model. A connection plate having a weight of 30N was attached on the raft with screws. Four load cells were set on the plate to measure vertical load on the raft, as shown in Figure 8.

In dynamic loading test, a vibro-hammer having a weight of 300N was placed on the raft. The vibro-hammer supplies the raft with not only the dead load but also dynamic load by rotating two discs having eccentric mass. Eccentricity of mass of each disc and input vibration frequency can control magnitude of the dynamic load. As shown in

Figure 9, the vibro-hammer can provide vibration load mainly in the vertical direction (called vertical loading) or in the vertical and horizontal directions simultaneously (called combination loading) by rotating discs synchronously in opposite directions or the same direction, respectively. Eccentric mass was kept constant in vertical loading and combination loading tests. Hence the amplitude of dynamic load depends on only the rotation frequency of the discs.

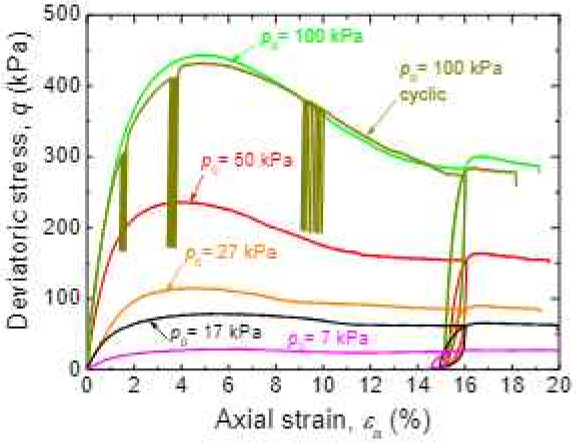

(a) Axial strain ε_a vs deviatoric stress q

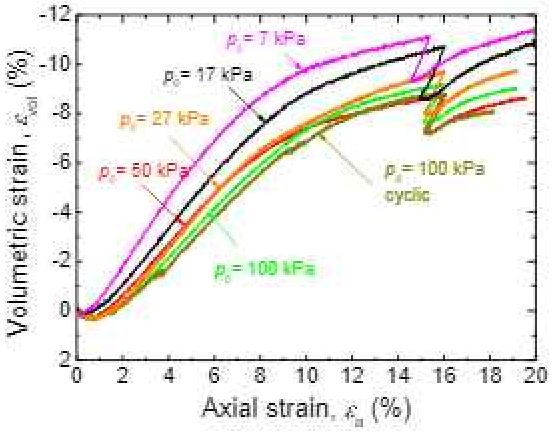

(b) Axial strain ε_a vs volumetric strain ε_{vol}

Figure 6 Results of triaxial CD tests for the sand (Vu et al, 2017)

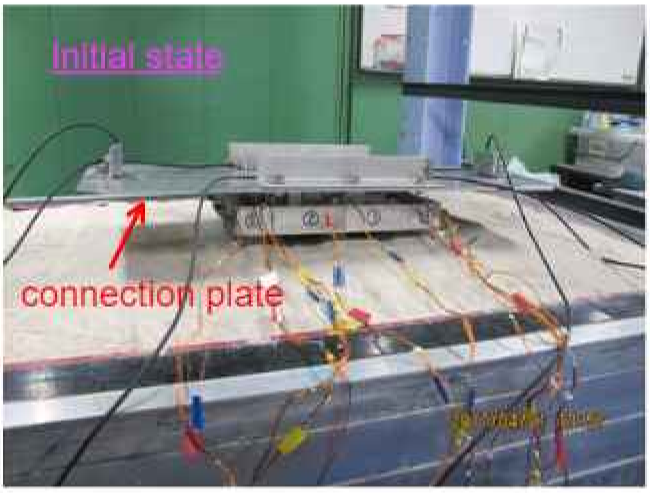

Figure 7 Pile foundation with connection plate

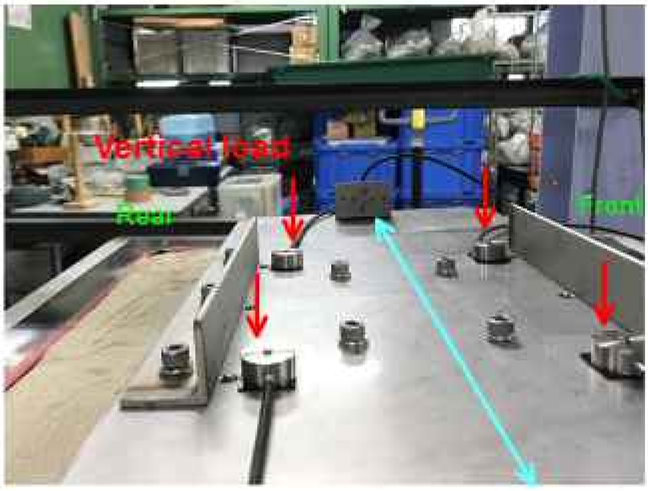

Figure 8 Setting load cells on connection plate

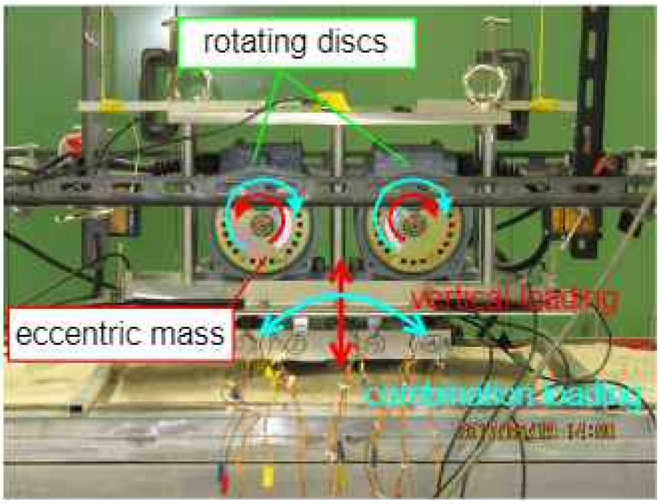

Figure 9 Loading mechanism by vibro-hammer

Figure 10 shows an illustration of experimental setup. Measurement transducers are accelerometer (Acc), laser displacement meter (Laser), encoder (ENC), load cell (LC), and strain gauges of each pile. Four accelerometers, from Acc1 to Acc4, are placed on the raft to measure the accelerations in the vertical and horizontal directions.

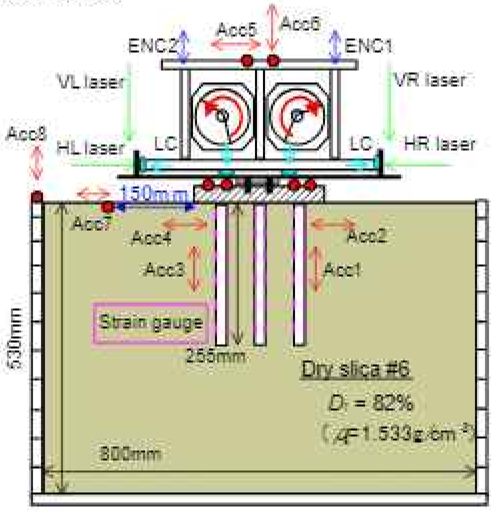

Figure 10 Experimental setup

2.4 Experimental cases

Figures 11 and 12 show experimental cases of each foundation model. In all the cases, firstly the foundation was vertically loaded using the self-weight of the vibro-hammer (Static loading test). Next, dynamic vertical loading test was carried out by operating the vibro-hammer. The input frequency, f, of the vibro-hammer was increased from 0 Hz to 30 Hz at intervals of 5 Hz.

In the cases of PG, when the settlement of the raft reached about 10 mm, vertical loading was interrupted. Thereafter, dynamic combination loading test was continued. In the cases of PR, dynamic combination loading test was conducted after the end of vertical loading test.

Apart from the dynamic loading tests mentioned above, sweep tests of each model foundation were carried out to estimate the natural frequency, f_n, of each model foundation. In the sweep tests, small amplitudes of vertical vibration was applied to the foundation using the vibro-hammer with increasing the rotation frequency. The response vertical acceleration of the raft was measured. The natural frequency of the foundation was obtained from the FFT processing of the measured response acceleration.

Figure 12 shows the natural frequency of each foundation model. The four foundation models have almost the same values (f_n = 14 to 15 Hz).

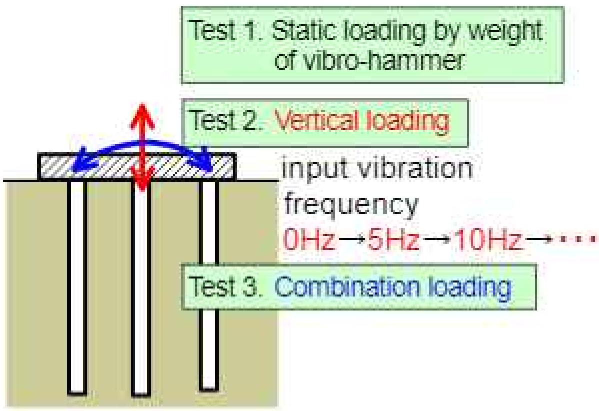

Figure 11 Experimental cases of each foundation model

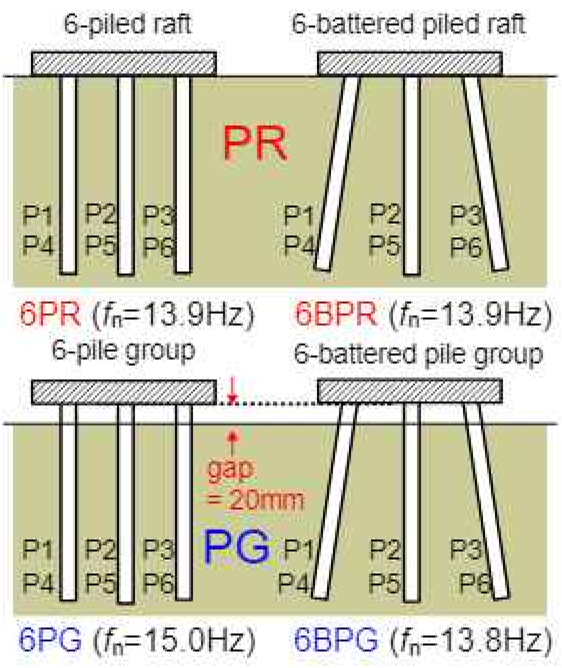

Figure 12 Natural frequency, f_n, of each foundation model

3. EXPERIMENTAL RESULTS

In this particular paper, the experimental results of dynamic vertical loading tests of 4 foundation models (6BPR, 6BPG, 6PR, 6PG) are presented and discussed.

3.1 Behaviours of each foundation model

Figure 13 shows changes of the vertical force, F_V (balck line), the horizontal force, F_H (blue line), and the input vibration frequency, f_v (pink line), with elapsed time, t, in the case of 6BPR.

The vertical load on the raft, F_V, was measured by the load cells (see Figure 8). The horizontal load, F_H, on the raft was inertial force calculated as the product of the horizontal acceleration and the mass of the vibro-hammer.

Although vertical loading was intended in these experiments, not only vertical load but also horizontal load acted upon the foundation model. It is thought that the horizontal load was caused by imperfect synchronization of two rotating discs having eccentric mass. As the result, combination load was applied to the raft.

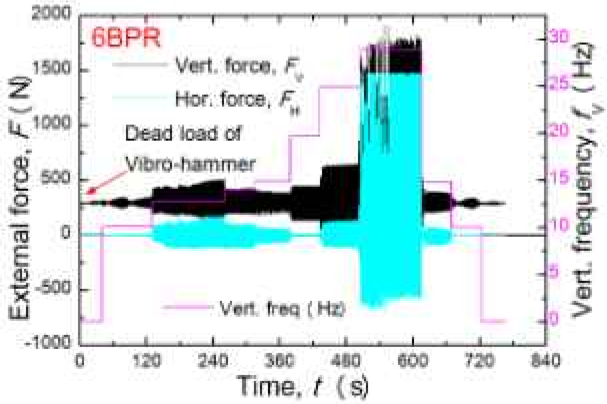

Figure 13 Time changes of input vibration frequency, f_V, vertical force, F_V, and horizontal force, F_H, in the case of 6BPR

Figure 14 shows changes of f_v and the vertical displacement, w, of the raft with elapsed time in the case of 6BPR. Note that the vertical displacement after the static loading by the self-weight of the vibro-hammer was set as 0. When f_v = 10 Hz, no vertical displacement occurred. This is reasonable, because the corresponding F_V was very small. When f_v was increased to 12 Hz, the vertical displacement started to occur and increased with time, and terminated at a certain time. Hence, f_v was further increased to 25 Hz, but the foundation was still stable without further increment of w. When f_v was increased to 30 Hz, the vertical displacement of the foundation started to increase suddenly. When f_v was decreased to 15 Hz, no more vertical displacement occurred.

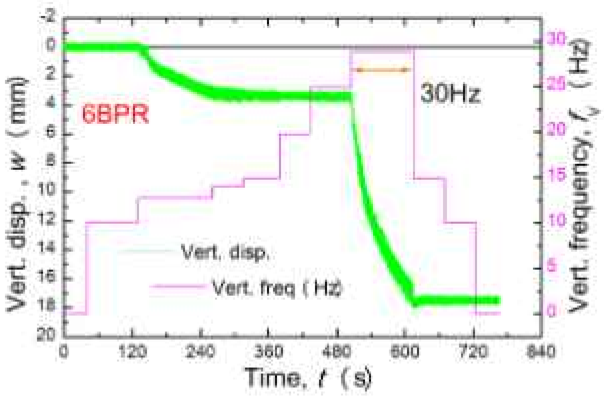

Figure 14 Time changes of input vibration frequency, f_V, and vertical displacement, w, in the case of 6BPR

The corresponding results in the cases of 6BPG, 6PR and 6PG are shown in Figures 15 to 20. The results of these cases were similar to those in 6BPR. In all the cases, the vertical displacement of the foundation started to increase rapidly when the input frequency, f_V, was increased to 30 Hz.

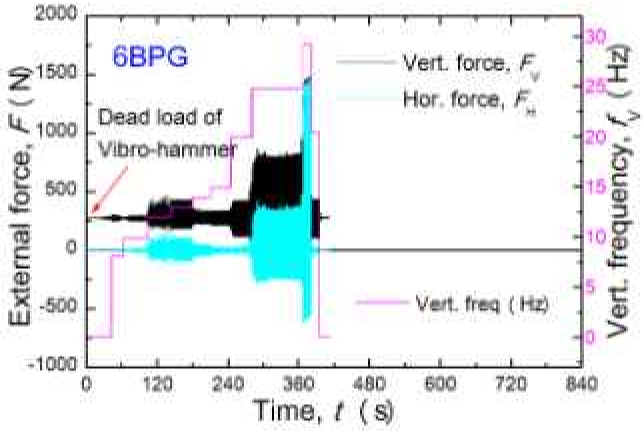

Figure 15 Time changes of input vibration frequency, f_V, vertical force, F_V, and horizontal force, F_H, in the case of 6BPG

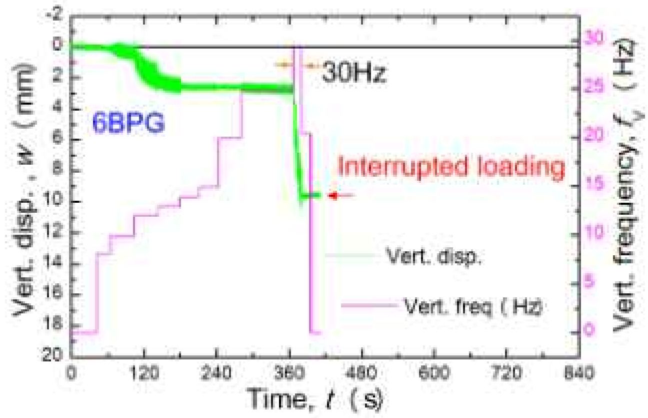

Figure 16 Time changes of input vibration frequency, f_V, and vertical displacement, w, in the case of 6BPG

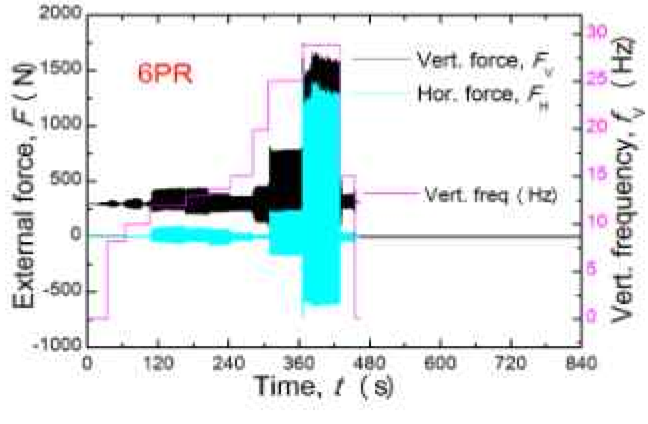

Figure 17 Time changes of input vibration frequency, f_V, vertical force, F_V, and horizontal force, F_H, in the case of 6PR

3.2 Comparisons of behaviours of the foundation models subjected to 30 Hz loading

In this section, the behaviours of each foundation model in loading step of f_V = 30 Hz are compared and discussed.

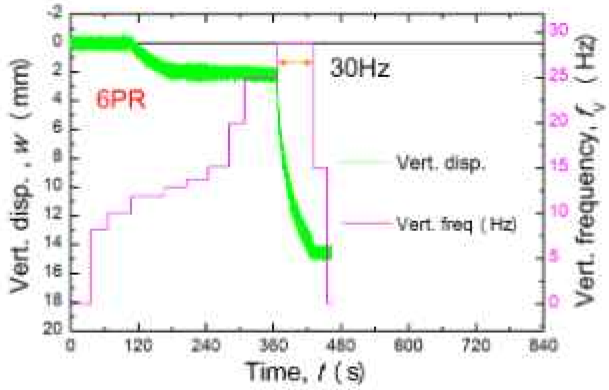

Figure 18 Time changes of input vibration frequency, f_V, and vertical displacement, w, in the case of 6PR

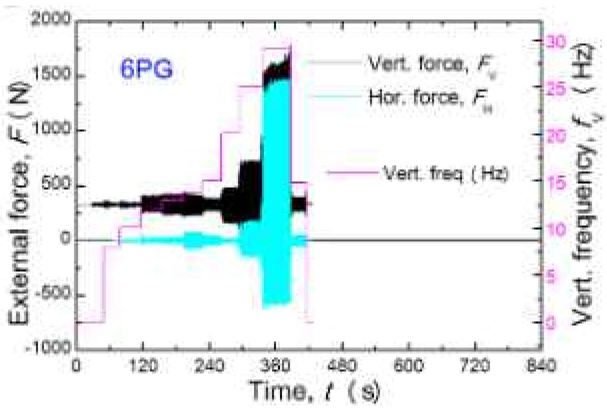

Figure 19 Time changes of input vibration frequency, f_V, vertical force, F_V, and horizontal force, F_H, in the case of 6PG

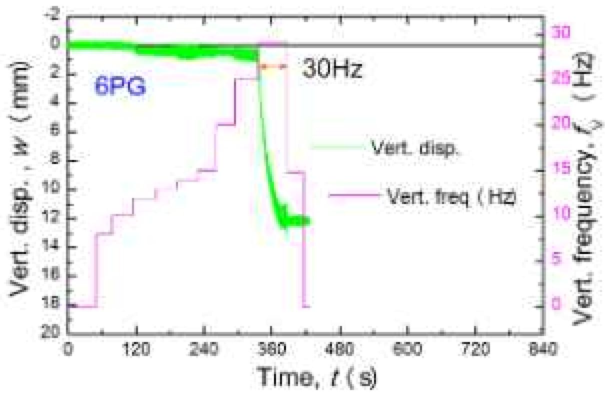

Figure 20 Time changes of input vibration frequency, f_V, and vertical displacement, w, in the case of 6PG

Figure 21 shows the vertical force, F_V, in each foundation model with elapsed time from the start of 30 Hz loading. Note that the vibro-hammer was placed on the raft but was not fixed to the raft. Hence, only compression but tension forces are generated during loading tests.

Figure 22 shows the increment of the vertical displacement, Δw, of each foundation with time from the start of 30 Hz loading.

Amplitudes of F_V in 6PR, 6PG and 6BPR were about 1600 N (Figure 21). The vertical displacement of 6BPR is the smallest followed by those of 6PR and 6PG, indicating that the batter piles and the raft base resistance suppress the vertical displacement. It may be judged from Figure 22 that inclusion of the batter piles is more effective to suppress the vertical displacement.

Although amplitudes of F_V in 6BPG were smaller than those in the other cases, Δw in 6BPG were comparable to those in 6PG. It is difficult to explain this result definitely at this stage.

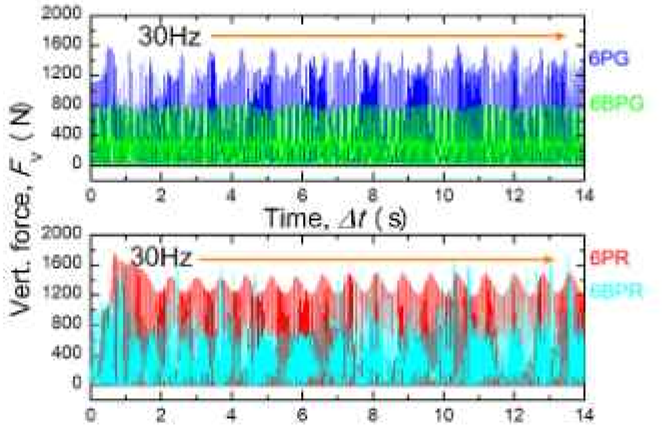

Figure 21 Time changes of vertical force, F_V, during 30 Hz loading

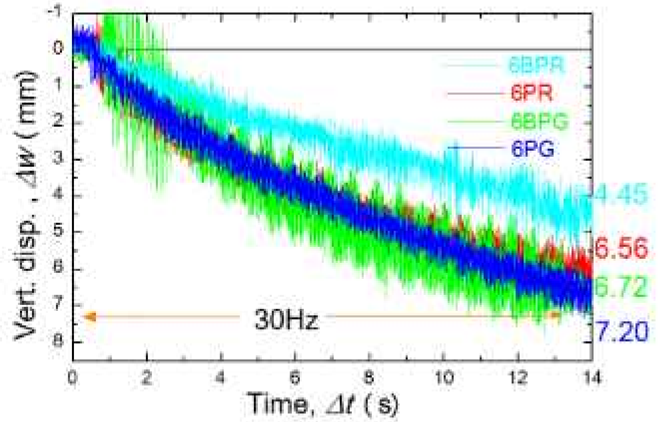

Figure 22 Increment of vertical displacement, Δw, of each foundation model with time during 30Hz loading

Figure 23 shows the increment of inclination of the raft, $\Delta\theta$, of each foundation model with time during 30 Hz loading. Comparison of $\Delta\theta$ in 6PG, 6PR and 6BPR indicates that the batter piles and the raft base resistance suppress the inclination of the foundation, similarly to the effect for suppressing the vertical displacement. The inclusion of the batter piles (6BPR) has a great effect on the inclination reduction of the foundation.

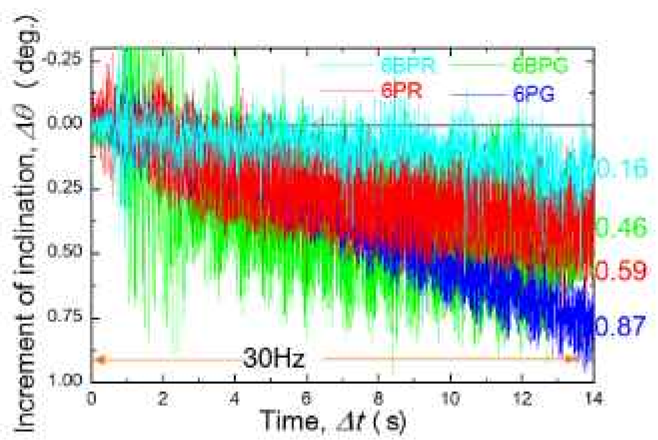

Figure 23 Increment of inclination, $\Delta\theta$, of each foundation model with time during 30Hz loading

Figure 24 shows the horizontal force, F_H, in the cases of 6BPR and 6BPG during 30 Hz loading. Amplitudes of F_H of 6BPG are larger than those of 6BPR. In contrast, amplitudes of vertical force, F_V, of 6BPG are smaller than those of 6BPR (see Figure 21). The larger amplitudes of F_H of 6BPG may be a reason for that the vertical displacement of 6BPG is relatively larger although amplitudes of F_V of 6BPG are smaller than the other cases.

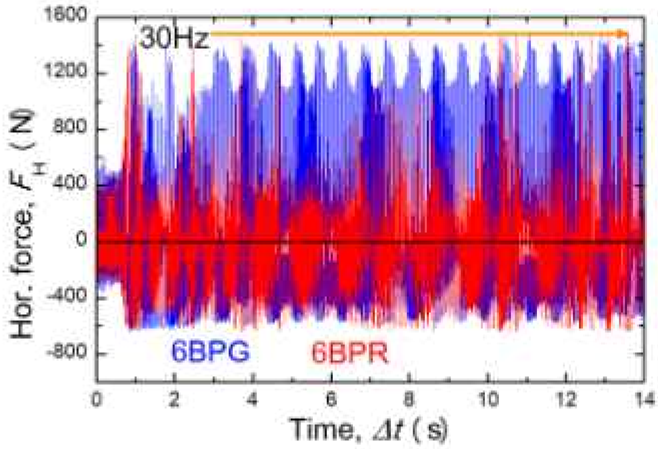

Figure 24 Time changes of horizontal force, F_H, during 30 Hz loading in cases of 6BPR and 6BPG

Figure 25 and Figure 26 show distributions of bending moments of the piles in 6BPR and in 6BPG, respectively, at elapsed time of 10s from the start of 30Hz loading. Bending moments of the piles in 6BPG are smaller than those in 6BPR, although horizontal forces on 6BPG are larger than those on 6BPR. Larger vertical load in 6BPR compared with that in 6BPG (see Figures 13 and 15) is one of the reasons that caused larger bending moments in 6BPR. Another reason could be the effect of load transferred from the raft base to the ground in the case of 6BPR. The load transferred to the ground increased stresses and stiffness of the soil beneath the raft, which resulted in larger bending moments in the piles of 6BPR.

It is also seen from Figures 25 and 26 that bending moments of the centre piles (P2 and P5) are very small in both of PR and PG.

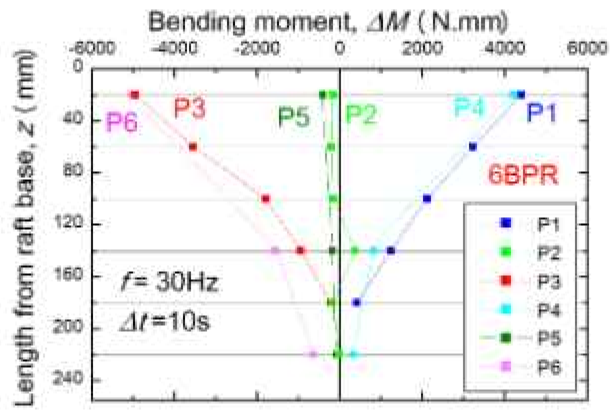

Figure 25 Distributions of bending moments of the piles in 6BPR at elapsed time of 10s from the start of 30Hz loading

Figure 27 and Figure 28 show horizontal accelerations of the vibro-hammer, the raft and the ground surface in shaking of 6BPR and in shaking of 6BPG, respectively, with elapsed time from the start of 30Hz loading. Horizontal acceleration on the raft of PR, Acc4 (Acc2 is almost equal to Acc4), is smaller than that of PG. This result indicates that raft base resistance is effectively mobilised to suppress the horizontal acceleration of the raft.

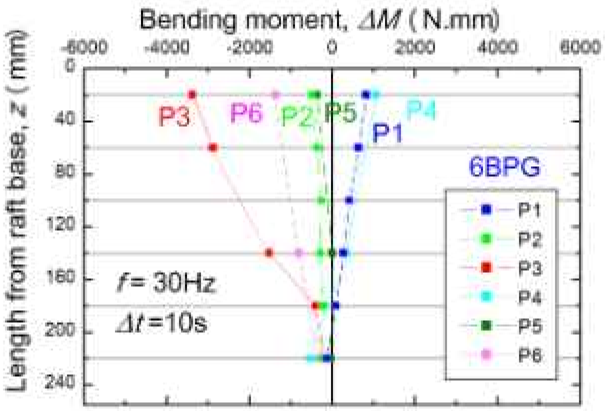

Figure 26 Distributions of bending moments of the piles in 6BPG at elapsed time of 10s from the start of 30Hz loading

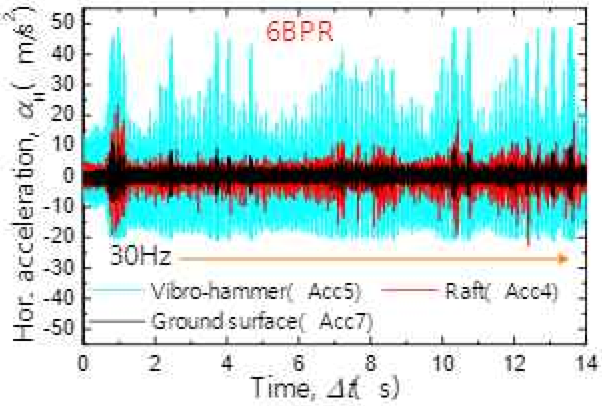

Figure 27 Horizontal accelerations of vibro-hammer, raft and ground surface in shaking of 6BPR with elapsed time from the start of 30Hz loading

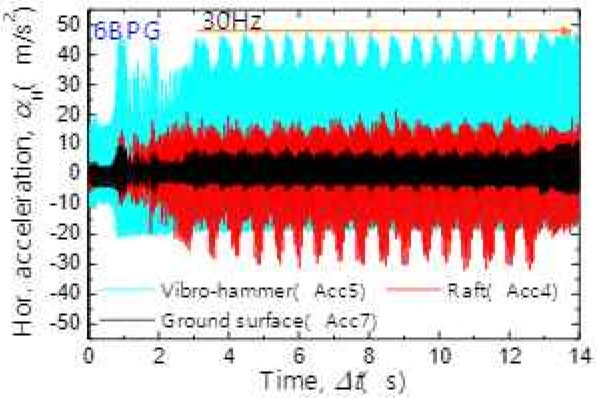

Figure 28 Horizontal accelerations of vibro-hammer, raft and ground surface in shaking of 6BPG with elapsed time from the start of 30Hz loading

Focusing on the ratio of horizontal acceleration at the ground surface to that on the raft, the ratio in PR is relatively higher than that in PG. This indicates that the influence of the shaking of the raft on the ground around PR is relatively larger than that around PG.

Similar result is found from the comparison of the experimental results of 6PR and 6PG, as shown in Figures 29 and 30.

A possible reason for this is illustrated in Figure 31. In the case of PR, the ground beneath around the raft is hardened by the raft base pressure. Hence, vibration of the raft is easily transmitted to the surrounding ground. In contrast, in the case of PG, the ground around the piles is softened by, for example, generation of gaps between the pile shaft and the ground. Therefore, the vibration of the surrounding ground is attenuated largely compared to that of the foundation.

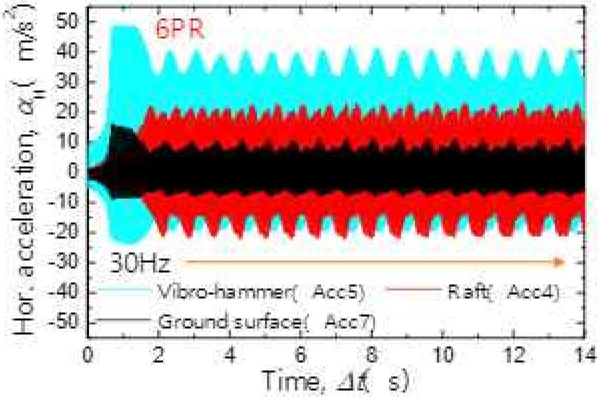

Figure 29 Horizontal accelerations of vibro-hammer, raft and ground surface in shaking of 6PR with elapsed time from the start of 30Hz loading

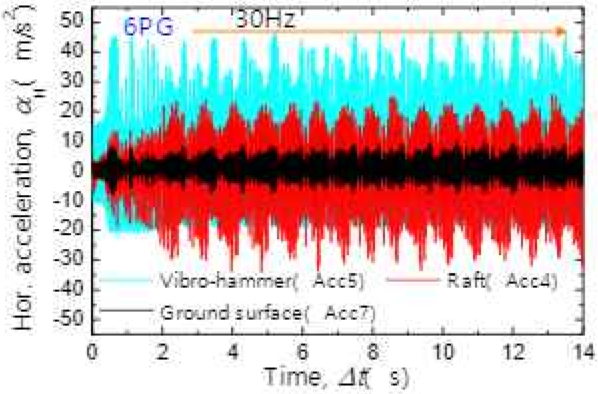

Figure 30 Horizontal accelerations of vibro-hammer, raft and ground surface in shaking of 6PG with elapsed time from the start of 30Hz loading

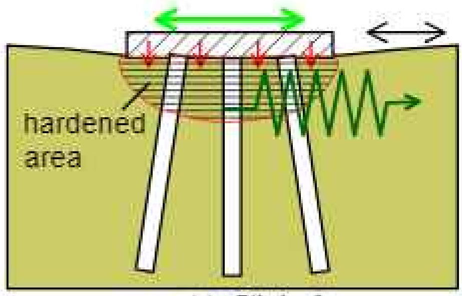

(a) Piled raft

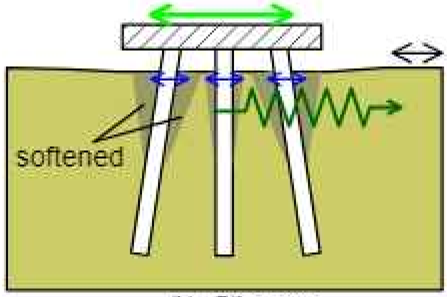

(b) Pile group

Figure 31 Illustrations of deformation patterns of the ground

4. CONCLUSION

Series of vibration load tests on 6-pile foundation models (with or without batter piles) in dry sand were carried out at 1-g field to investigate the behaviours the foundations.

The experimental results indicate that the piled rafts are more effective than the pile groups in suppressing vertical displacement and inclination induced by vertical dynamic load. It is also confirmed from the results that piled raft with batter piles is the most effective type to reduce settlement and inclination.

Behaviour of piled raft and pile group foundations in saturated sand subjected to vibration is a future study.

5. REFERENCES

Ghasemzadeh, H., and Alibeikloo, M. (2011) "Pile soil pile interaction in pile groups with batter piles under dynamic loads". Soil Dynamics and Earthquake Engineering, 31, pp1159-1170.

Goit, CS., and Saitoh, M. (2013) "Model tests and numerical analyses on horizontal impedance functions of inclined single piles embedded in cohesionless soil". Earthquake engineering and engineering vibration, 12, pp143-154.

Hamada, J., Tsuchiya, T., Tanikawa, T., and Yamashita, K. (2015) "Lateral loading tests on piled rafts and simplified method to evaluate sectional forces of piles". Geotechnical Engineering Journal SEAGS & AGSSEA, 46(2), pp29-42.

Horikoshi, K., Matsumoto, T., Hashizume, Y., Watanabe, T., and Fukuyama, H. (2003) "Performance of piled raft foundations subjected to static horizontal loads". Int. Jour. of Physical Modelling in Geotechnics, 3(2), pp37-50.

Isam, S., Hassan, A., and Mhamed, S. (2012) "3D elastoplastic analysis of the seismic performance of inclined micropiles". Computers and Geotechnics, 39, pp1-7.

Katzenbach, R., Arslan, U., and Reul, O. (1998) "Soil-structure-interaction of a piled raft foundation of a 121 m high office building on loose sand in Berlin". In Proceedings of Deep Foundation on Bored and Auger Piles, pp215-221.

Ko, J., Cho, J., and Jeong, S. (2017) "Nonlinear 3D interactive analysis of superstructure and piled raft foundation". Engineering structures, 143, pp204-218.

Matsumoto, T., Fukumura, K., Pastsakorn, K., Horikoshi, K., and Oki, A. (2004) "Experimental and analytical study on behaviour of model piled rafts in sand subjected to horizontal and moment loading". International Journal of Physical Modelling in Geotechnics, 4(3), pp1-19.

Poulos, H.G. and Davids, A.J. (2005) "Foundation design for the Emirates Twin Towers, Dubai". Canadian Geotechnical Journal, 42, pp716-730.

Poulos, H.G., and Small, J.C., Chow, H. (2011) "Piled raft foundations for tall buildings". Geotechnical Engineering Journal SEAGS & AGSSEA, 46(2), pp78-84.

Randolph, M. F. (1994) "Design methods for pile groups and piled rafts". Proc. 13th ICSMGE, Vol. 5, New Delhi, pp. 61-82.

Reul, O. (2004) "Numerical study of the bearing behaviour of piled rafts". International Journal of Geomechanics, 4(2), pp59-68.

Sadek, M., and Isam, S. (2004) "Three dimensional finite element analysis of the seismic behaviour of inclined micropiles". Soil Dynamics and Earthquake Engineering 24: 473-485.

Sawada, K., and Takemura, J. (2014) "Centrifuge model tests on piled raft foundation in sand subjected to lateral and moment loads". Soils and Foundations, 54(2), pp126-140.

Unsever, Y.S., Matsumoto. T., Shimono, S., and Ozkan, M.Y. (2014) "Static cyclic load tests on model foundations in dry sand". Geotechnical Engineering Journal SEAGS & AGSSEA, 45(2), pp40-51.

Unsever, Y.S., Matsumoto, T., Esashi, K. and Kobayashi, S. (2017) "Behaviour of model pile foundations under dynamic loads in saturated sand". Bulletin of Earthquake Engineering, 15(4), pp1355-1373.

Vu, A.T., Matsumoto, T., Kobayashi, S., and Shimono, S. (2017) "Experimental study on pile foundations having batter piles subjected to combination of vertical and horizontal loading at 1-g field". Geotechnical Engineering Journal SEAGS & AGSSEA, 48(3), pp12-24.

Vu, A.T., Matsumoto, T., Kobayashi, S., and Nguyen, T. L. (2018) "Model load tests on battered pile foundations and finite-element analysis". International Journal of Physical Modelling in Geotechnics, 18(1), pp33-54.

Yamashita, K., Yamada, T., and Hamada, J. (2011) "Investigation of settlement and load sharing on piled rafts by monitoring full-scale structures". Soils and Foundation, 51(3), pp513-532.

Watcharasawe, K., Kitiyodom, P., and Jongpradist, P. (2017) "Investigation 3-D Numerical analysis of consolidation effect on piled raft foundation in Bangkok subsoil condition". International Journal of Geomate, 12(31), pp105-111.